The Pharma Innovation Journal 2022; 11(6): 1068-1072

www.ThePharmaJournal.com

The Pharma Innovation

ISSN (E): 2277-7695
ISSN (P): 2349-8242
NAAS Rating: 5.23
TPI 2022; 11(6): 1068-1072

www.thepharmajournal.com
Received: 07-02-2022
Accepted: 16-05-2022

Shivanand
Ph.D., Department of Dairy Engineering Division, Southern Regional Station, ICAR-National Dairy Research Institute, Bengaluru, Karnataka, India

F Magdaline Eljeeva Emerald
Principal Scientist, Department of Dairy Engineering Division, Southern Regional Station, ICAR-National Dairy Research Institute, Bengaluru, Karnataka, India

Somveer
M.Tech., Department of Dairy Engineering Division, Southern Regional Station, ICAR-National Dairy Research Institute, Bengaluru, Karnataka, India

Corresponding Author:
Shivanand
Ph.D., Department of Dairy Engineering Division, Southern Regional Station, ICAR-National Dairy Research Institute, Bengaluru, Karnataka, India

Synthesis and characterization of aluminum oxide nanoparticles

Shivanand, F Magdaline Eljeeva Emerald and Somveer

Abstract
Nano-sized alumina oxide (Al_2O_3) nanoparticles (NPs) have been successfully synthesized by chemical precipitation method using aluminum nitrate as precursor and citric acid as reducing agents. Precipitation method of synthesizing Al_2O_3 is most efficient and simplest process using inexpensive raw materials, produces less pollution, and has several advantages such as purity, thermal stability and homogeneous nanoparticle in size. The synthesized NPs have been characterised by UV-vis, SEM, FTIR, AFM and XRD. Result of UV-vis and FTIR confirms the formation of aluminum oxide NPs. XRD peaks show the grain size of aluminum oxide NPs. Scanning electron microscopy (SEM) reveals that the particle size of the particles lies between 30 and 90 nm.

Keywords: Nanoparticles, SEM-EDX, FTIR, AFM, XRD, UV-vis, nanofluids

1. Introduction
Alumina is a prominent substance in industrial applications and from a technological standpoint. Alumina NPs are utilized in many areas of modern industry such as electronics, metallurgy, optoelectronics and fine ceramic composites. Nanofluids (NFs) are the dispersion of nano-sized particles in a base fluid and in recent time these are applied as potential heat transfer fluid, which was termed after the innovative studies by Choi *et al.* (1995) [1]. Very small sizes and large specific areas of the NPs, enables NFs to have superior properties like high thermal conductivity, minimal clogging in flow passages, long-term stability, and homogeneity compared with base fluids. Characteristics of NFs like stability and thermo-physical properties are the performance indicators in a heat transfer system like minichannel. In nanofluids preparation NPs used which are basically metal (Cu, Al, etc.), metal oxides (Al2O3, TiO2, CuO, SiO2, etc.) and some other compounds (CNT, TNT, graphene, etc.). Base fluids usually include water, ethylene glycol, refrigerant, engine oil, and others.
Lee *et al.* (1999) [2] reported that NFs provide better heat transfer characteristics because of their high surface area that facilitated heat transfer. They offer many advantages: 1) high specific surface area of metal NPs provides more heat transfer surface between particles and fluids 2) high heat dispersion stability with predominant Brownian motion of particles that remains stable for months because of stabilising agent present in it 3) enhancement of thermal conductivity 4) enhancement of conductivity was achieved with a very small concentration of particles 5) enhancement of thermal conductivity was found to depend not only on particle concentration but also on particle size. In general, with decreasing particle size, an increase in enhancement was observed.
Nanofluids are fluid NPs suspensions that exhibit enhanced properties at modest NP concentrations. Nanofluids have unique heat transfer properties and are utilized in high heat flux systems (e.g., electronic cooling systems, heat exchanger liquids, solar collectors, and nuclear reactors). However, suspension stability is critical in the development and application of these heat transfer fluids. Reynolds number, mass concentration, and particle size control the heat transfer behavior of fluids
The preparation of well-dispersed and stable NFs is seen as a challenging job. Due to high interaction between the particles, they tend to undergo agglomeration which in turn causes a reduction in thermal conductivity and clogging of channels in PHE. To prepare well dispersed and stable NFs, many techniques have been researched of which one-step and two-step methods are considered suitable for preparation of metal oxide NFs. In one-step method, physically evaporated metal vapours are directly condensed into the base fluids in a vacuum chamber (Eastman *et al.*, 2001; Lo *et al.*, 2005) [3, 4].

This method produces highly stable and efficient NFs but the production cost is higher with lower capacity. In two-step method, NPs are first produced in dry powder form using physical or chemical techniques. The nanosized powder is then dispersed in base fluid by applying intensive agitation by means of magnetic force or high-shear or ultrasonic agitation or ball milling or homogenising. Two-step method is believed to be most economical method to prepare NFs at large scale as the nanopowder synthesis has already been scaled up to industrial level. Due to the high surface area and surface activity, NPs have the tendency to aggregate. The important technique to enhance the stability of NPs in fluids is the use of surfactants. However, the functionality of the surfactants under high temperature is also a big concern, especially for high temperature applications.

2. Materials and Methods

2.1 Procurement of chemicals

Citric acid ($C_6H_8O_7$) and aluminum nitrate nonahydrate (Al $(NO_3)_3.9H_2O$) was purchased from Hi media and Merck, respectively.

2.2 Synthesis of aluminum oxide nanoparticles

The Al_2O_3 NPs were synthesized by the following process (Saleh and Gupta, 2012). The aluminum nitrate and citric acid were used as precursor. The concentrations of aluminum nitrate and citric acid were 0.5 M. The aluminum nitrate nonahydrate [Al $(NO_3)_3.9H_2O$] of 18.75 g and citric acid [$C_6H_8O_7$] of 9.606 g were dissolved in 100 mL distilled water of two separate beakers. The solutions were thoroughly mixed with glass rod to ensure the complete dissolution of salts. The beaker containing [Al $(NO_3)_3.9H_2O$] solution was placed over a hot plate cum magnetic stirrer (Model: C-MAG HS7, IKA Werke GmbH & Co.KG, Staufen, Germany) maintained at 80°C. The citric acid solution was transferred into burette and added slowly drop by drop to [Al $(NO_3)_3.9H_2O$] solution. The solution was stirred constantly for 8 h at a temperature of 80°C, until it colour become yellowish sol. Than sample rapidly heated to 100°C and stirred constantly. The temperature of the system was then increased up to 200°C and kept for 3 h until a fluffy, polymeric citrate precursor was obtained. It was then allowed to dry and then it was ground to a fine powder. Then the contents were transferred into a porcelain dish and kept in muffle furnace (Model: Culture Instruments, Bengaluru, India) for calcinations process at 800°C for 3 h.

2.3 Characterisation of aluminum oxide nanoparticles

2.3.1 X-ray diffraction (XRD)

XRD is an analytical technique commonly used for identification of crystalline materials, examination of the unit cell sizes and crystal structure. Each particle produces a unique signature of X-ray. The X-ray pattern shows the X-ray intensity versus scattering angle that is characteristic of its crystalline atomic structure. Qualitative analysis is possible by comparing the XRD pattern of an unknown material to a library of known patterns. For both qualitative and quantitative analysis of crystalline compounds, therefore, XRD is one of the most powerful techniques. The technique gives insight about type and nature of phase present, micro strain, size, degree of crystallinity, orientation and amount of amorphous content. The Al_2O_3 NPs were analysed with powder X-ray diffractometer (Model: Rigaku SmartLab, Tokyo, Japan) using Cu-Kβ radiation source (λ=0.139 nm) at 40 kV and 30 mA with goniometer speed of 0.02 s^{-1}. In the range of 30-70° the diffractograms were measured for 2θ. The crystallite sizes (D) were calculated by Debye-Scherrer's formula (Eq. 2) (Cullity, 1967) [5].

X-rays incident upon a crystal is scattered in different ways. When the wavelength of the radiation (λ) is comparable to the atomic spacing in a crystal, the scattering which is termed as diffraction, gives rise to a set of well defined beams arranged with a characteristic geometry, thus forming a diffraction pattern. X-ray diffraction data collection is the result of relative intensity (I) for each reflection with a set of planes in the crystal, designated by Miller indices (h k l), along with the corresponding scattering angle (2θ) for that reflection. The positions and intensities of the diffracted beams are a function of the arrangements of the atoms in space and some other atomic properties. A beam of radiation will only be diffracted when it imposed upon a set of planes in a crystal if the geometry of the situation fulfills quite specific law defined by Bragg‟s known as Bragg‟s law (cullitiy, 1978) [6].

$$n\lambda = 2d_{hkl}\sin\theta \quad (1)$$

Where

'n' is order of diffraction
'λ' is wavelength,
'd' is the interplanar spacing of hkl planes in crystal lattice
'θ' is Bragg angle

Average crystallite size (L) of NPs were calculated by "Scherrer Formula"

$$L = \frac{K\lambda}{\beta\cos\theta} \quad (2)$$

Where, 'K' is Scherrer's constant in the range 0.87 – 1.0, 'λ' is wavelength of the radiation, 'β' is full width at half maximum (FWHM) of the peaks, 'θ' is Bragg angle

2.3.2 Scanning electron microscopy-energy dispersive X-ray analysis (SEM-EDX)

Scanning electron microscopy (SEM) is a technique where minute sample may be used to determine particle size, shape, and texture. In SEM a fine beam of electrons scan across the prepared sample in a series of parallel tracks. The electrons interact with the sample, and produce several different signals which can be detected and displayed on the screen of a cathode ray tube. Particles less than 1 nm can be viewed, and since the depth of focus is so much greater than that of the light microscope, information on surface texture can be generated. The surface morphology of Al_2O_3 NPs was examined by scanning electron microscope (Model: GEMINI Ultra 55, Zeiss, Jena, Germany). Sample was coated with sputter gold coating of thickness 5 to 10 nm (Model: Q150R ES, Quorum Technologies Ltd., Kent, England). The morphology of Al_2O_3 NPs was obtained at different magnifications of 5, 10, 25 and 50 kX with an acceleration voltage of 5.0 kV. Energy dispersive X-ray spectroscopy (Model: X-Max 150, Oxford Instruments, Wiesbaden, Germany) is an analytical technique used for the analysis of elemental composition.

2.3.3 UV-visible spectroscopy

Energy absorbed in the UV region produces changes in the electronic energy of the molecule. The optical properties of Al_2O_3 NPs were find out using UV-vis double beam spectrophotometer (Model: UH5300, Hitachi High Technologies, Tokyo, Japan). Initially distilled water was used as blank (control). Exactly 0.1 g of Al_2O_3 NPs were dispersed in 100 mL of distilled water and mixed using high shear homogeniser for 30 min to prepare stock solution. The standard solution was prepared by taking 9 mL from stock solution and the volume was adjusted to 30 mL using distilled water. The standard solution was vortexed for 5 min and UV-vis absorption spectrum of the Al_2O_3 NPs absorbed at particular wavelength was noted.

The relationship between the energy absorbed (E) in an electronic transition and the frequency (ν), wavelength (λ) of the radiation producing the transition is given by (Eq. 3)

$$\Delta E = h\nu = hc/\lambda \quad (4)$$

Where, h=Planck's constant c=velocity of light, ΔE=energy absorbed in an electronic transition in a molecule

Determination of the optical energy gap using Tauc formula (Eq. 4)

$$\alpha h\upsilon = B(h\upsilon - E_g)^n \quad (5)$$

n=1/2 for direct band gap and n=2 for indirect band gap. Where, α is absorption coefficient. With the help of band gap is α determined. We plot the photon energy hυ vs $(\alpha h\upsilon)^2$ and hυ vs $(\alpha h\upsilon)^{½}$ for direct and indirect band gap respectively. By fitting a straight line to this plot. The constant term of its equation is equal to E_g

2.3.4 Fourier Transform Infrared Spectroscopy (FTIR)

The FTIR spectra of Al_2O_3 NPs were recorded using Fourier transform infrared spectrometer (Model: Perkin Elmer Frontier, Singapore). Exactly 5 mg of Al_2O_3 NPs was mixed with potassium bromide (KBr: Al_2O_3 NPs 95:5) and the mixture was then compressed into pellet form. To eliminate any noise in the spectrum, each spectrum was recorded at a resolution of 4 cm^{-1} with an average of 32 scans/min. The scanning range of wavenumber varied from 650 to 4000 cm^{-1}.

2.3.5 Atomic force microscopy (AFM)

Surface roughness of Al_2O_3 NPs was determined using atomic force microscope (Model: Scan Asyst, Bruker Corporation, Santa Barbara, USA). Sample was prepared by mixing 2 mg of NPs in 100 mL of isopropyl alcohol. The mixture was ultrasonicated for 40-50 min and from that one drop of sample was drop casted on a clean glass slide and was dried under vacuum for 72-75 h. The dried sample was analysed for surface characteristics such as mean surface roughness and roughness kurtosis in an area of 1×1 micron at a scan rate of 1.0 Hz.

3. Results and Discussion

3.1 Synthesis of aluminum oxide nanoparticles

The detailed synthesis method of aluminum oxide NPs depicted in Fig 1. In this method, the following chemical reaction takes place and Al_2O_3 is formed

$$6Al(NO_3)_3 \cdot 9H_2O + 5C_6H_8O_7 \rightarrow 3Al_2O_3 + 74H_2O + 30CO_2 + 9N_2$$

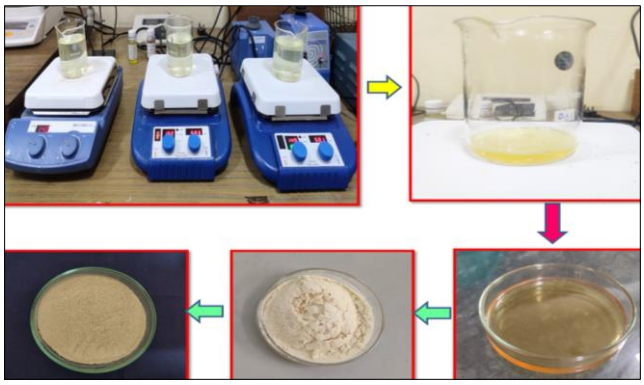

Fig 1: Synthesis of aluminum oxide nanoparticles

3.2 Characterisation of aluminum oxide nanoparticles

3.2.1 Powder X-ray diffractometry

The Al_2O_3 NPs synthesised by chemical precipitation process were characterised for phase identification and their purity. The XRD pattern of Al_2O_3 NPs was recorded (Fig. 2) and from the diffractogram, the characteristic spectral peaks obtained at 2θ values of 13.57°, 30.82°, 37.25°, 42.29° and 65.3°. Based on Debye Scherrer equation (Eq. 2) the average crystallite size of synthesised NPs was 24.19 nm.

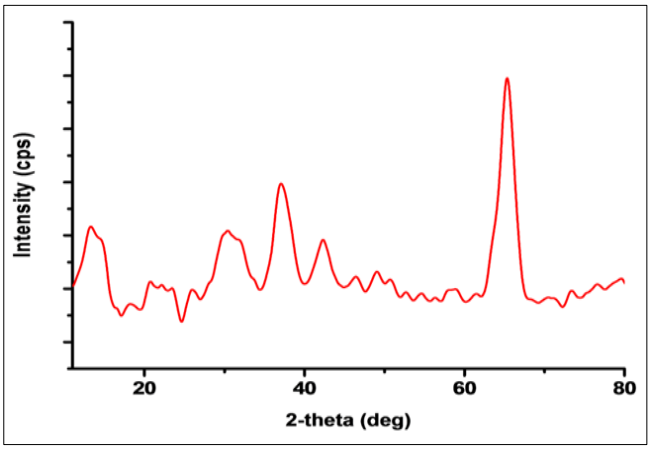

Fig 2: X-ray Diffractogram of synthesised aluminum oxide nanoparticles

3.2.2 Scanning electron microscopy-energy dispersive X-ray spectroscopy

The SEM photographs of Al_2O_3 NPs at 10 to 100 kX magnifications are shown in Fig. 3. Surface morphology of Al_2O_3 NPs shows flakes-like and has uniform size and distribution. The flake-shaped particles were uniformly distributed throughout materials with the average size in the submicron range. The sheer size might be in several micrometre levels which we can clearly notice in SEM image. Overall, SEM images reveal that the sheet-like morphology of Al_2O_3 NPs might be enhanced the overall performance of the NFs. Similar micrographs were obtained for the Al_2O_3 NPs by Prashanth *et al.* (2015) [7]. The elemental composition of the synthesised Al_2O_3 NPs is further confirmed by EDX analysis for the presence Al/O. From the Fig. 4, Al_2O_3 NPs, Al contains 30.54 at%, O contains 64.27 at% respectively.

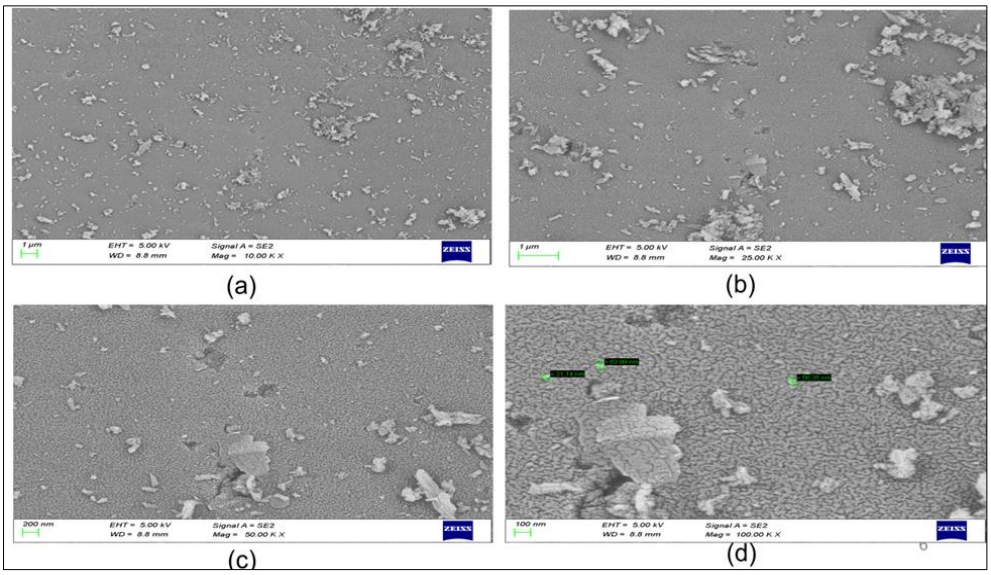

Fig 3: SEM micrographs of synthesised aluminum oxide nanoparticles at magnification of 10 kX (a), 25 kX (b), 50 kX (c) and 100 kX (d)

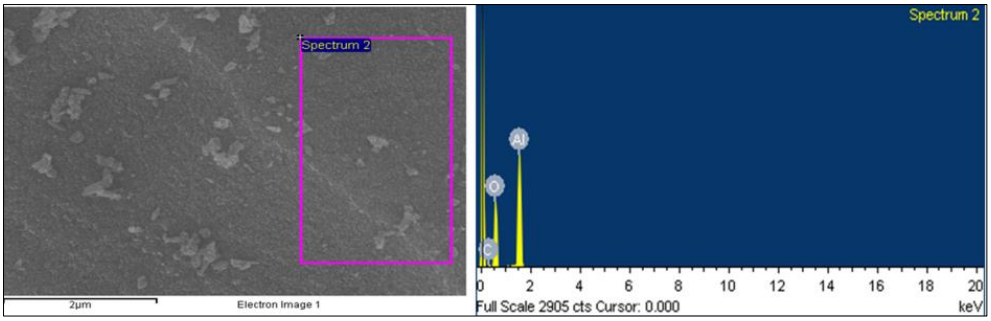

Fig 4: SEM-EDX of synthesised aluminum oxide nanoparticles

3.2.3 UV-visible spectroscopy

The UV-vis absorption spectrum was recorded in order to determine the optical energy band gap of sample. The sample shows a strong absorption peak (λ_{max}) at 207 nm in the UV region which confirms the formation of Al_2O_3 particles. Prashanth *et al.* (2015) [7] obtained the strong absorption peak between the 200 to 250 (238) nm in the uv region for Al_2O_3 NPs. These values are in agreement with Koopi and Buazar (2018) [8] (227 nm). Similarly, Kumar *et al.* 2021[9] reported 210 nm maximum absorption peak verifies the presence of the Al_2O_3 NPs and in agreement with the present recorded data of 207 nm absorption peak value. Jwad *et al.* 2019 [10] recorded maximum absorption peak of 220 nm for Al_2O_3 NPs synthesized by laser ablation method. At 240 nm a strong absorption peak had been clearly confirms the formation and presence of Al_2O_3 NPs in deionized water reported by Al-Jawad *et al* (2015) [11]. Fig. 5a depicts the UV-vis absorption spectrum of sample. This can be attributed to photoexcitation of electron from valence band to conduction band. The optical energy band gap (E_g) was estimated (Fig. 5b) by the method proposed by Wood and Tauc 1972 [12] according to the equation (Eq. 4). The E_g value of Al_2O_3 is 5.4. This value is good aggrement with the E_g of 5.25 eV reported by the Prashanth *et al.* (2015) [7]. Similarly, Koopi and Buazar (2018) [8] obtained optical energy band gap (Eg, eV) value of 5.46 eV for Al_2O_3 NPs.

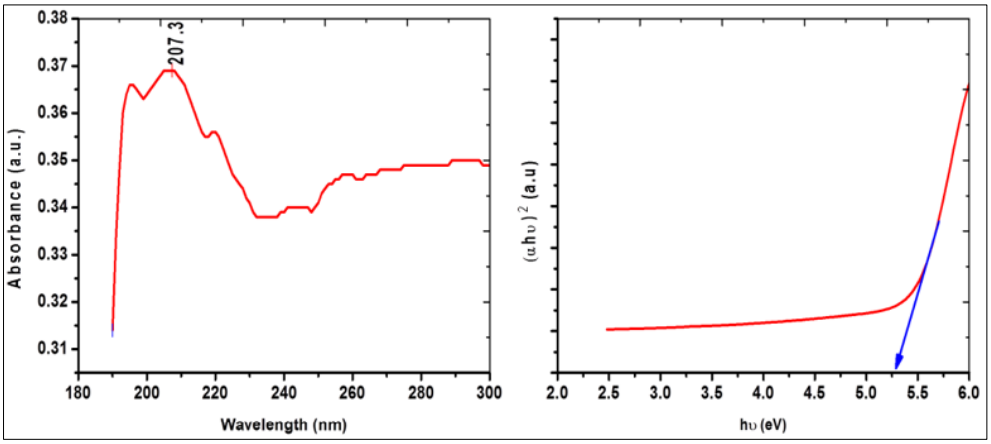

Fig 5a: UV-vis spectrum and 5b Tauc plot of synthesised aluminum oxide nanoparticles

3.2.4 Fourier-transform infrared spectroscopy

The FTIR spectrum of the synthesised Al_2O_3 NPs obtained in the range of 650-4000 cm^{-1} (Fig. 6). Strong absorption bands in the 659–931 cm^{-1} range can be assigned to the stretching vibration of Al-O bond which confirmed the formation of the Al_2O_3 NPs. A weak band can be seen at 1941-2293 cm^{-1} which is attributed to the stretching vibration of the C-H bond. The broad absorption peak between 2680-3670 CM^{-1} may be attributed to O-H vibration of water. Around at 1313-1444 CM^{-1} corresponds to the Al-OH bonding mode, as can be seen, this peak disappears by increasing the heat treatment.

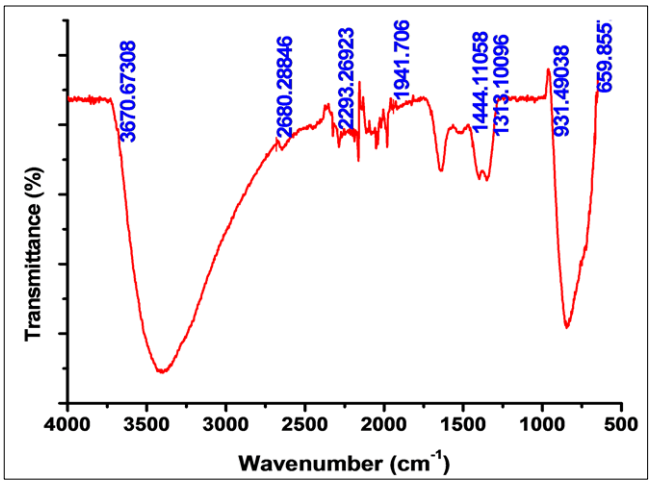

Fig 6: FTIR spectrum of synthesised aluminum oxide nanoparticles

3.2.5 Atomic force microscopy

Fig. 7a depicts the two-dimensional view (2D view), while Fig. 7b depicts the three-dimensional view (3D view) of AFM image of synthesised Al_2O_3 NPs. The mean roughness of synthesised Al_2O_3 NPs was 117.611 nm, indicated that the distribution was uniform and the homogeneity was strong within the scanning field. The roughness kurtosis (R_{ku}) was 4.868 indicated that the distribution had comparatively greater number of high peaks and low valleys with spiky surface.

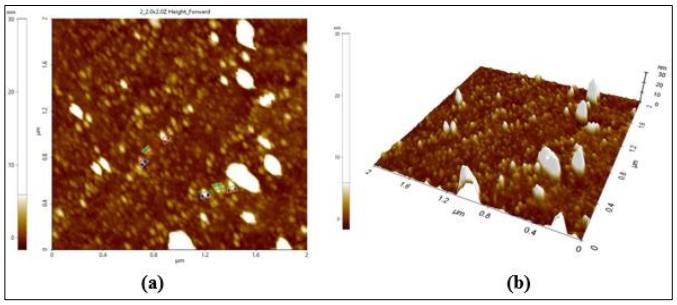

Fig 7: AFM Images of synthesised aluminum oxide nanoparticles a) 2D and b) 3D Views

4. Conclusion

Precipitation is the most efficient method for synthesizing Al_2O_3. It is the simplest compared to other methods, has low raw material costs, produces no pollution, and has several advantages such as high purity products, nearly homogeneous NPs in size, excellent thermal conductivity, and controlling desired particle size. The results of the study help in producing Al_2O_3 NPs. Further research is needed to determine the most effective materials and efficient procedure in using the precipitation method.

5. References

1. Choi SU, Singer DA, Wang HP. Developments and applications of non-Newtonian flows. Asme Fed. 1995;66:99-105.
2. Lee S, Choi SS, Li SA, Eastman JA. Measuring thermal conductivity of fluids containing oxide nanoparticles. Journal of Heat transfer. 1999;121(2):280-289.
3. Eastman JA, Choi SU, Li S, Yu W, Thompson LJ. Anomalously increased effective thermal conductivities of ethylene glycol-based nanofluids containing copper nanoparticles. Applied physics letters. 2001;78(6):718-20.
4. Lo CH, Tsung TT, Chen LC. Shape-controlled synthesis of Cu-based nanofluid using submerged arc nanoparticle synthesis system (SANSS). Journal of Crystal Growth. 2005;277(1-4):636-42.
5. Cullity BD. Elements of X-ray diffraction. Addison Wesely Publishing Company Inc., Massachusetts, USA, 1967, 342.
6. Cullity BD. Elements of X-Ray diffraction. In Elements of X-ray diffraction (Second.). Addison-Wesley Publishing Company, Inc, 1978, 664.
7. Prashanth PA, Raveendra RS, Hari Krishna R, Ananda S, Bhagya NP, Nagabhushana BM, *et al*. Synthesis, characterizations, antibacterial and photoluminescence studies of solution combustion-derived α-Al2O3 nanoparticles. Journal of Asian Ceramic Societies. 2015;3(3):345-51.
8. Koopi H, Buazar F. A novel one-pot biosynthesis of pure alpha aluminum oxide nanoparticles using the macroalgae Sargassum ilicifolium: a green marine approach. Ceramics International. 2018;44(8):8940-5.
9. Kumar H, Gehlaut AK, Gupta H, Gaur A, Kamsonlian S, Kumar D. Facile synthesis and application of aluminum oxide nanoparticle based biodegradable film. Polymer Composites. 2021;42(8):3899-910.
10. Jwad KH, Saleh TH, Abd-Alhamza B. Preparation of Aluminum Oxide Nanoparticles by Laser Ablation and a Study of Their Applications as Antibacterial and Wounds Healing Agent. Nano Biomed. Eng. 2019;11(3):313-9.
11. Al-Jawad SM, Al-Algawi SD, Khalef WK. Characterization of laser-ablated nanostructured Al2O3/p-Si solar cells. Iraqi Journal of Applied Physics, 2015, 11(1).
12. Wood DL, Tauc JS. Weak absorption tails in amorphous semiconductors. Physical review B. 1972;5(8):3144.